JOURNAL OF SPACECRAFT AND ROCKETS
Vol. 29, No. 3, May-June 1992

# Thermal Distortion Analysis of an Antenna-Support Truss in Geosynchronous Orbit

Jeffery T. Farmer,* Deborah M. Wahls,† and Robert L. Wright*
*NASA Langley Research Center, Hampton, Virginia 23665*
and
A. Louis Tahernia‡
*TRW, Inc., Washington, D.C. 20546*

**The effects of the geosynchronous thermal environment on the surface accuracy of a tetrahedral-truss support structure for a high-frequency microwave antenna concept for Earth-science monitoring have been studied. The thermal environment and the slow rotation of the spacecraft relative to the Sun result in long exposure to both heating and cooling conditions and, consequently, in severe temperature extremes. Resulting transient temperatures ranged from 150 to −180°C and were strongly influenced by the shadow cast by the reflector surface. The use of truss element surface coatings achieved mixed success in alleviating thermal problems. Multilayer insulation or a Sun shield worked best in reducing surface distortions, but the distortions still exceeded the required surface accuracy. Surface accuracy requirements could only be met by customization of surface coatings and element expansion characteristics.**

## Nomenclature

$D$ = diameter of antenna
$f$ = focal length of antenna
$lf$ = length fraction of both end fittings to total element length
$\alpha$ = absorptivity of material
$\epsilon$ = emissivity of material
$\lambda$ = wavelength of operating frequency

## Introduction

MULTI-INSTRUMENT spacecraft in geosynchronous orbit will provide scientific data to support NASA's Global Change Technology Initiative. A spacecraft (Fig. 1) that could support a variety of Earth-observing instruments with widely diverse pointing requirements while providing a stable, stiff platform for pointing accuracy has been developed.[1] Two passive microwave radiometers, with antenna diameters of 15 and 7.5 m, are deployed at opposite ends of the spacecraft. Data accuracy is strongly dependent on the structural distortion of the spacecraft and the surface accuracy of the large antennas. A thermal-distortion analysis of the 7.5-m-antenna support structure and the spacecraft box truss and a structural dynamic analysis of the low-frequency microwave radiometer (15-m diam) antenna have been conducted.[2,3]

In this study, a thermal-distortion analysis has been conducted on the truss support structure for the high-frequency microwave sounder (7.5-m diam) antenna. Distortions due to external loading or manufacturing errors are not addressed. Several thermal control approaches to reduce temperatures and thermal gradients in the structural elements are investigated, including truss element thermal coatings, multi-layer insulation, a Sun shield, and advanced low-thermal-expansion materials. Performance of the thermal control techniques in reducing surface distortions on the reflector is assessed.

## Antenna Description

The high-frequency microwave sounder (HFMS) uses an offset-fed Cassegrain antenna with a focal-length-to-diameter ratio ($f/D$) of 1.5 for high-quality measurement and scanning (Fig. 2). It consists of a parabolic primary reflector and supporting truss structure, a subreflector, feed, a feed support beam, and associated electronic data gathering, processing, and distribution equipment. For the present study, the components of interest are the primary reflector and supporting truss.

### Primary Reflector

The HFMS primary reflector has a 7.5-m diam (typical of the size that might be employed) and a highly accurate surface. Estimates of the required reflector surface accuracy,[4,5] ranging from $\lambda/50$ to $\lambda/100$, where $\lambda$ is the wavelength (cm) of the highest operating frequency (220 GHz), suggest a maximum allowable rms surface error between 0.0136 mm (0.53 mil) for $\lambda/100$ and 0.027 mm (1.06 mil) for $\lambda/50$. An accuracy value of 0.0136 mm (0.53 mil) is used for comparison purposes. This accuracy dictates the use of a moderate-precision solid surface; however, the reflector's diameter (7.5 m) compared with the size of the available launch alternatives (i.e., 4.4 m for the Shuttle Orbiter) suggests some form of segmented reflector that can be deployed or assembled on orbit. The segmented reflector in this study is composed of a set of highly polished reflector surface panels individually supported at the joints of a tetrahedral truss structure designed for on-orbit assembly. The reflector panels are fabricated of a graphite or glass composite honeycomb structure. The front surface is coated with aluminized Kapton to provide the required high radio frequency (rf) reflectivity and to minimize the temperature excursions and resulting distortions of the panels. The back surface of the antenna (the side facing the platform) is covered with multilayer insulation (MLI) to control heat transfer to and from the panels.

Received June 9, 1990; presented as Paper 90-1673 at the AIAA/ASME 5th Joint Thermophysics and Heat Transfer Conference, Seattle, WA, June 18-20, 1990; revision received Sept. 9, 1991; accepted for publication Sept. 9, 1991. 

*Aerospace Technologist, Space Station Freedom Office.
†Aerospace Technologist, Vehicle Analysis Branch, Space Systems Division. Member AIAA.
‡Systems Engineer.

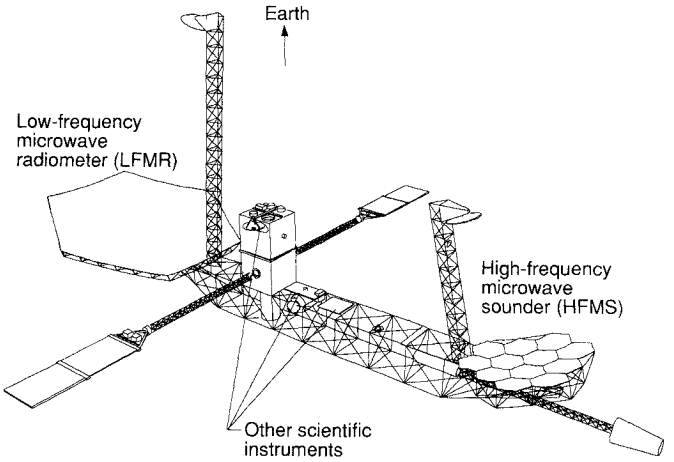


**Fig. 1 Geostationary Earth-science platform.**

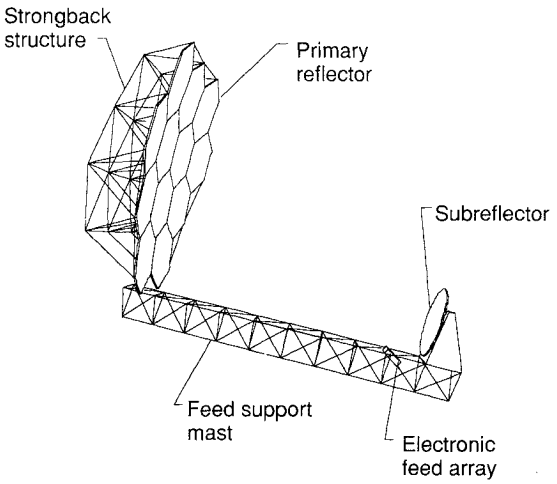


**Fig. 2 7.5-m-diam high-frequency microwave sounder.**

### Support Structure

The main function of the support structure is to provide stable support to minimize distortions in the overall shape of the reflector. The tetrahedral truss concept was selected for its advanced level of development, design heritage, and lightweight, high-strength characteristics. This truss must precisely maintain relative positions and orientations of the individual panels with respect to the feed and the other panels. The baseline tetrahedral-truss structure is composed of thin (2.5-cm diam with 3-mm-thick walls) tubes of uncoated P75 graphite/epoxy composite, with aluminum joints.[6] Thermophysical properties of the tubes are given in Table 1.

Since each structural element consists of both tubes and joints, the element coefficient of thermal expansion (CTE) is based on the CTE of both components and the ratio of joint length to the total length of the element:

$$CTE_{eff} = CTE_t + lf(CTE_j - CTE_t)$$

where $CTE_{eff}$ is the effective element CTE, $CTE_t$ the tube CTE, $CTE_j$ the joint CTE, and $lf$ the length fraction (total length of both joints divided by the entire element length). For the baseline concept, the tubes are fabricated of unidirectional P75 graphite ($CTE = -1.08 \times 10^{-6}$ cm/cm/°C), each with two aluminum joints ($CTE = 23.4 \times 10^{-6}$ cm/cm/°C), resulting in a length fraction of 12.2% and an element CTE of $1.9 \times 10^{-6}$ cm/cm/°C. The solar absorptivity to thermal emissivity ($\alpha/\epsilon$) ratio is close to unity; alternative coatings with $\alpha/\epsilon$ ratios less than and greater than unity are also considered.

The material properties and structural integrity of some candidate graphite composites may vary or degrade at elevated temperatures (above 100°C), but many thermoplastic composites are cured at higher temperatures and can withstand temperatures higher than the 100°C level. Thus, the properties listed earlier are assumed not to vary with temperature, and the 100°C level is used as a guideline for comparison.

## Modeling and Analysis

The thermal and structural analyses were performed using the following computer-aided engineering software: Tetrahedral Truss Structural Synthesizer[7] (finite element model development), Supertab[8] (visual inspection and modification of finite element models and postprocessing of results), Thermal Model Generator[9] (thermal modeling and analysis), Model Solution[10] (linear static structural analysis), and Antperf[11] (parabolic shape changes).

### Thermal Analysis

Thermal analyses were performed to determine element temperature variations for the uncoated graphite truss under two orbit conditions. Effectiveness of element surface coatings, multilayer insulation, and a Sun shield were examined as means of reducing temperature excursions and improving surface accuracy. Analyses included formulation of thermal models based on the finite element model, selection and quantification of heating conditions, and calculation of truss element temperatures for the baseline and alternate thermal control concepts.

#### *Thermal Model*

The thermal model used for determining internal heat transfer in this analysis consists of the truss structure and the solid reflector surface. Each truss element and joint is assumed isothermal. The reflector is modeled using triangular thin-shelled elements that approximate the thermal characteristics of a honeycomb panel. The reflector is included in the analysis to assess its impact on the thermal behavior of the truss. The modes of heat transfer in the model are conductive and radiative coupling, with the primary mode being radiative.

Most of the internal heat transfer in the model occurs through radiation between the reflector and the individual truss elements. Heat transfer among truss elements (whether by conduction or radiation) is quite small. No conduction is assumed between the reflector panels and the truss. View factors between the truss elements and the reflector elements (the percentage of heat leaving one surface that is incident on another) is on the order of 0.1. More important, the low solar absorptivity (thus, high solar reflectivity) of the MLI results in large amounts of reflected solar energy impinging on the truss elements and elevating their temperatures during already hot conditions. During a portion of the orbit, the reflector shades the truss elements, preventing any type of heating and allowing their temperatures to drop to severely low levels. This shadowing effect occurs every orbit and is relatively independent of the Sun's declination. Shadowing by the truss elements is also included in the analysis but has a much less significant impact.

The radiative coupling between elements depends primarily on the view factors of the elements and their thermal emissivity and solar absorptivity. The view factors between the truss

**Table 1 Thermophysical properties of uncoated P75 graphite composite tubes**

| | |
|---|---|
| Young's modulus, N/m | $2.7 \times 10^{11}$ |
| Mass density, kg/m$^3$ | 1740 |
| Specific heat, J/kg-°C | 850 |
| Thermal conductivity, W/m-°C | 76 |
| Coefficient of thermal expansion,cm/cm/K | $-1.08 \times 10^{-6}$ |
| Solar absorptivity ($\alpha$) of surface | 0.9 |
| Thermal emissivity ($\epsilon$) of surface | 0.8 |

elements are on the order of 0.001 or smaller, resulting in low radiative coupling. When thermal coatings are applied to the elements, the resulting heat transfer becomes negligible when compared with that between the reflector panels and the truss elements.

*Thermal Environment*

The thermal environment experienced in geosynchronous orbit is defined by the external radiative heat fluxes from the Sun and Earth, the space heat sink, the existence and length of eclipse periods, and the internal heat exchanges. External heat sources include incident solar radiation, solar radiation reflected from Earth (solar albedo), and incident Earth radiation (Earth thermal). Solar albedo and Earth thermal radiation depend on distance from the Earth and are insignificant

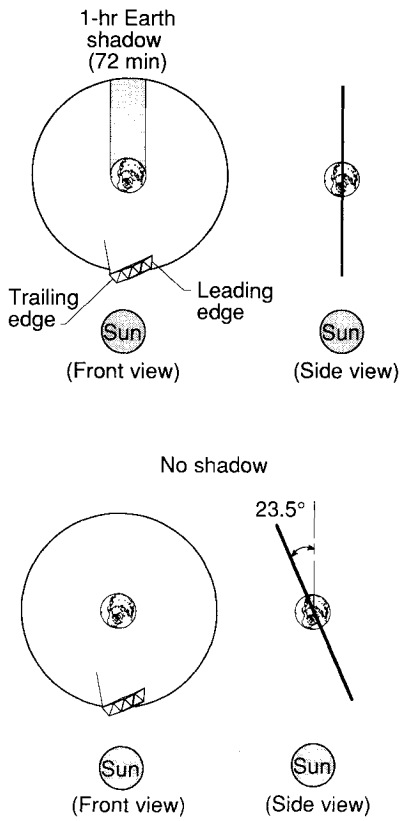


**Fig. 3 Description of equinox and solstice orbits.**

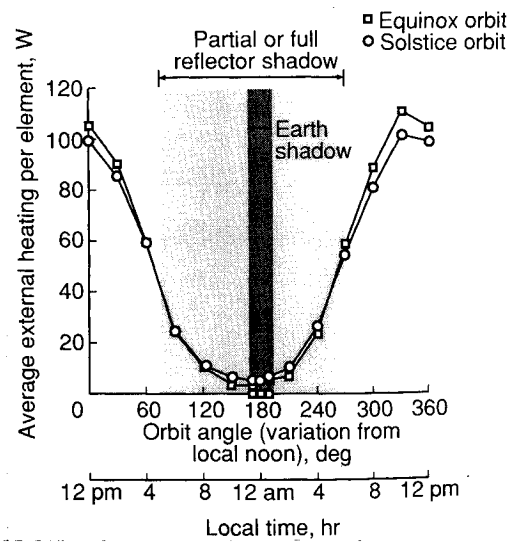


**Fig. 4 Average external heat input variation with orbit position.**

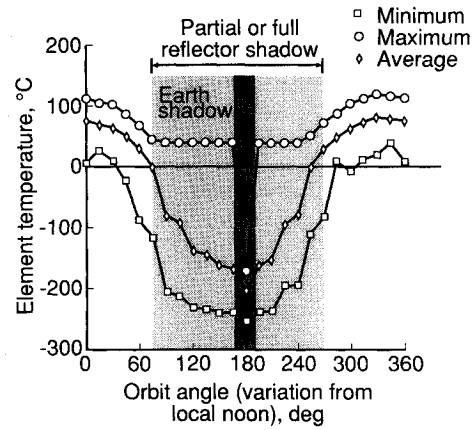


**Fig. 5 Equilibrium (steady-state) temperature variation with orbit position for uncoated truss elements—equinox orbit.**

(less than 1% of the total heating) at geosynchronous altitude when compared to solar heating. Truss cooling is induced by cold space (assumed to be a black body at 4 K) and by eclipses each orbit during equinox seasons. The slow rotation of the reflector and truss support relative to the Sun (characteristic of a geosynchronous Earth-oriented body) results in long exposure to both heating and cooling and, consequently, in severe temperature extremes.

In order to bracket the thermal environmental extremes, the thermal analysis considered two orbits (Fig. 3): one occurring during equinox (which includes a 72-min eclipse) and the other occurring during solstice (no eclipse).

*External Heating Rates*

External heating rates (primarily direct solar radiation) are calculated on each truss element at 12 orbital positions. For the equinox orbit, additional heating rates are calculated just before and after entering and exiting the Earth's shadow. Figure 4 shows the orbital variation of external heating rates averaged over all of the truss elements for both the equinox and solstice orbits beginning at 0 deg (where the antenna is directly between the Sun and the Earth).

As the truss support progresses through its orbit, the orientation of the individual elements relative to the solar radiation can vary between parallel, producing minimal heating, and perpendicular, producing maximum heating. The distribution of the element orientations causes severe local temperature gradients and distortions that can adversely impact antenna performance.

The truss elements also receive a large amount of solar radiation reflected from the back of the reflector during periods when the back of the reflector is oriented toward the Sun. The solar radiation striking some elements is almost doubled during these periods. The offset nature of the antenna concept (Fig. 2) causes this doubling to occur at an orbit position near solar noon. As the back of the reflector points away from the Sun, the reflected solar energy and resulting rate of heating decreases substantially, as shown in Fig. 4 for both orbit cases. In the solstice case (Fig. 3), a tilt angle exists between the orbit plane and the Sun vector. This tilt reduces the energy striking the reflector and, consequently, the reflected energy and heat by the sine of the tilt angle, resulting in lower average heat fluxes than in the equinox case during Sun periods.

Reflector blockage begins at an orbit angle of approximately 75 deg and noticeably reduces heating on the elements. This reduced heating is similar in magnitude for both orbits and occurs during every orbit. The slight tilt of the solstice case keeps more of the elements from being shaded by the reflector than in the equinox case. The solstice cases retain slightly higher average heating values that occur between orbit angles of 120 and 250 deg. The effect of the Earth's shadow

can be seen on the equinox heating curve as the small but sharp drop occurring around 180 deg.

Although the temperature variations are similar for both orbits, the more extreme heating and cooling of the equinox orbit produce a more diverse thermal environment and greater thermal distortions. Consequently, the equinox orbit was selected as the worst case and all results presented here are based on this case unless otherwise specified.

*Temperature Characteristics of Baseline Concept*

Temperatures were computed for each element in each orbital position for use in the distortion analysis. Average element temperatures were then calculated for each orbital position. Figures 5 and 6 show the variation in this average element temperature through an equinox orbit for steady-state and transient conditions, respectively, along with the corresponding minimum and maximum temperatures along the truss at each orbit position.

Wide temperature variations are experienced by the truss elements, ranging from 115 to $-250$°C for the steady state and from 115 to $-160$°C for the transient analysis. The difference in temperature between the hottest and coldest elements at each orbit position also varies significantly, to a maximum of 190°C. As the average and minimum temperatures drop, the maximum temperature remains relatively constant. (This maximum is the hottest temperature in the truss, which does not necessarily occur at the same element for each orbit position.) The effect of the Earth's shadow can be seen by the sharp drop and ensuing rise in maximum element temperatures occurring around 180 deg. However, the sharp drop is less for the steady-state minimum and average temperatures (Fig. 5) and does not occur for the transient minimum and average temperatures (Fig. 6). The average temperature decreases gradually as more of the elements move into the shadow of the reflector at orbit positions from approximately 75 to 180 deg. As the elements exit the reflector shadow (about 180 deg), the average element temperature rises more gradually than the maximum. The steady-state temperatures are helpful for understanding more about the environment at a given orbit position by representing equivalent sink temperatures. However, these results can provide misleading information about both the temperatures the elements actually experience and also where the worst conditions exist. For instance, the steady-state maximum temperature difference across the truss is 290°C and occurs at positions of 165 and 195 deg, whereas the transient maximum temperature difference of 190°C occurs at 240 deg. The transient values are representative of actual temperatures and are therefore used to determine surface distortions, which are proportional to temperature difference. Note that using the 290°C (steady-state) difference would lead to excessively large distortion estimates.

*Temperature Characteristics of Alternative Thermal Protection Techniques*

In addition to distorting the truss and degrading antenna performance, high temperatures can also deteriorate the antenna structural materials. At temperatures above 100°C, some graphite composites can begin to decompose, leading to catastrophic failure in the truss. Maximum temperatures calculated during Sun periods of the orbit exceed this value (Fig. 6). Consequently, some form of thermal protection is needed to prevent these high temperatures and possibly reduce the resulting surface distortions. Three methods of protecting the truss structure were examined: 1) directly coating each structural element with a thin surface coating that is integral to the structure, 2) wrapping each element with MLI, and 3) enclosing the entire truss structure within a Sun shield.

*Coating.* An etched-aluminum coating fabricated directly on the graphite tubes has surface properties, i.e., solar absorptivity $\alpha$ and infrared emissivity $\epsilon$, that can be adjusted during fabrication by controlling the etching process. Two coatings with different $\alpha/\epsilon$ values were considered in this analysis: a

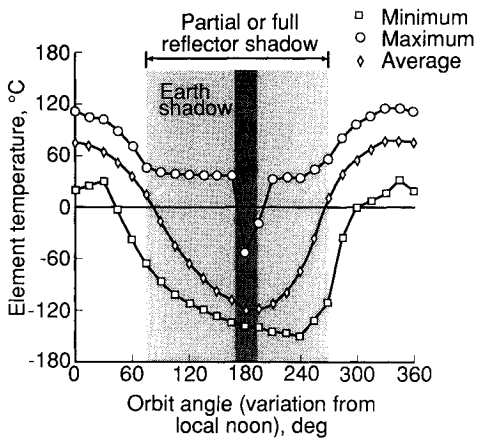


**Fig. 6 Transient temperature variation with orbit position for uncoated truss elements—equinox orbit.**

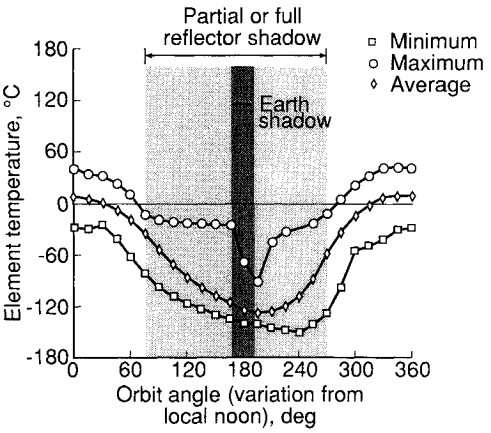


**Fig. 7 Transient temperature variation with orbit position for low-ratio ($\alpha/\epsilon$ = 0.3/0.65) coated elements—equinox orbit.**

low-ratio (0.3/0.65) coating and a high-ratio (0.3/0.2) coating. Minimum, maximum, and average transient temperatures are presented in Figs. 7 and 8 for each of the two surface coatings. In Fig. 7 (the low $\alpha/\epsilon$ ratio case), a desirable decline in all of the element temperatures occurred at orbit positions around 0 deg. This decline is attributed to the more favorable heat balance set up by the low $\alpha/\epsilon$ ratio. The lower absorptivity reduces the amount of heat absorbed by the element, and the higher emissivity allows more of the heat absorbed from the Sun to be rejected to space, reducing all temperatures. The reduced temperature variation across the truss at each orbit angle helps to reduce surface distortions.

The high $\alpha/\epsilon$ ratio coating concept also reduces the temperature across the truss, but its lower emissivity restricts heat rejection and results in temperatures well above the 100°C level during Sun periods (Fig. 8). During the shade period, this restricted heat rejection allows the coolest element temperatures to remain more elevated than in the low-value case, which helps to reduce the surface distortions.

The coated element analysis indicates that both coatings produce more desirable results than the uncoated case, but they still have associated problems. These results indicate that a surface having a low $\alpha/\epsilon$ ratio ($< 1.0$) for sunlight operation while having a low emissivity ($\sim 0.2$) for night or shadow operation would be the ideal surface. However, coatings with these properties, which will meet the long mission times and be easily producible, are not readily available.

*Multilayer insulation.* An alternative to these coatings is to individually wrap each element in a sleeve of MLI. The sleeve is made of thin layers of highly reflective material separated by nonconductive meshes. This sleeve provides a

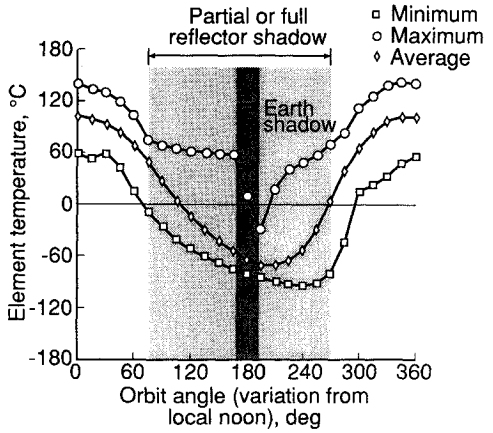


**Fig. 8 Transient temperature variation with orbit position for high-ratio ($\alpha/\epsilon = 0.3/0.2$) coated elements—equinox orbit.**

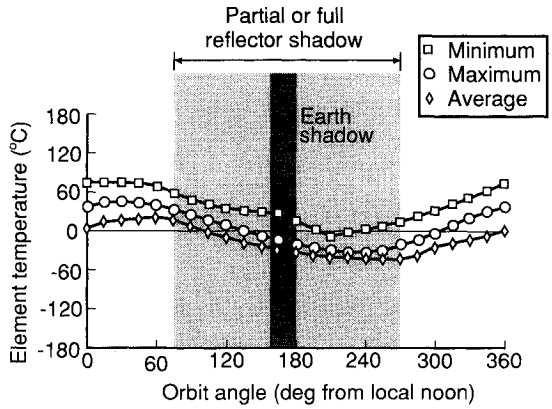


**Fig. 9 Transient temperature variation with orbit position for the truss elements wrapped in multilayer insulation—equinox orbit.**

radiation shield around each element that tends to decouple the elements from the environment, effectively lowering both the solar absorptivity and infrared emissivity. The MLI sleeve was modeled by changing both the absorptivity and emissivity of each element to 0.05, giving an $\alpha/\epsilon$ ratio of 1.0.

The temperature profile for the MLI (Fig. 9) is very similar to the coating profiles; however, the temperature excursion throughout the orbit is greatly diminished. The maximum temperature is 74°C, well below the suggested maximum temperature limits, and, therefore, should pose no threat to the material integrity of the struts. The minimum temperatures are above −43°C, and the temperature difference at any given orbit position is fairly small, which helps minimize resulting structural distortions. One disadvantage is that the MLI-covered struts require extra care in packaging and assembly to prevent damage to the insulation.

*Sun Shield.* Enclosing the entire truss structure in a Sun shield provides an alternative method for decoupling the individual structural elements from their environment. This prevents any direct exposure of the elements to both the Sun and cold space, thus reducing heat gain and loss by the truss as a whole and the variation in external heating across the truss. The Sun shield was assumed to be 1-mm-thick aluminized Kapton with $\alpha/\epsilon$ ratios of 0.35/0.6 on the outside and 0.3/0.2 on the inside. The temperature profile for the Sun shield is shown in Fig. 10. Since the Sun does not directly impinge on the elements, the maximum temperatures are lower than all of the previous cases. Additionally, the cold temperatures that occur during reflector shadowing remain relatively higher since the elements are viewing the warmer Sun shield rather than cold space. This concept prevents degradation of the structural integrity of the material by maintaining temperatures well within the material limits. It also reduces possible distortions by preventing element temperatures from radically falling or rising during shaded periods and by maintaining small temperature gradients across the truss.

*Comparisons.* Figure 11 provides a comparison of the average element temperatures for the baseline (uncoated) and the four thermal protection alternatives. The average temperature profiles from Figs. 6–10 are combined in Fig. 11 to better compare the effect of each thermal design on truss temperatures. For instance, both coated concepts have less severe temperature variations through an orbit than does the uncoated concept. The low-ratio (0.3/0.65) coating maintains low temperatures during the sunlit periods, whereas the low-emissivity of the high-ratio coating reduces heat loss during shaded periods, thus keeping temperatures from reaching severely cold levels. The Sun shield and the MLI maintain moderate temperatures during both sunlight and shaded portions of the orbit. As expected, the temperature swings for these two options are the smallest of those considered and are approximately equal. The MLI temperature profile is slightly elevated from that of the Sun shield by virtue of its extremely small emissivity value of 0.05, which significantly restricts rejection of heat.

The mean standard deviation in temperature as a function of orbit position (Fig. 12) is an estimate of the actual temperature variation across the truss, which, when combined with Fig. 11, is an indication of the severity of the thermal distor-

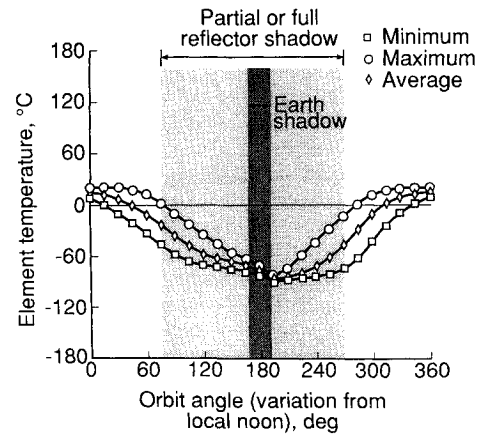


**Fig. 10 Transient temperature variation with orbit position for the truss elements enclosed in a Sun shield—equinox orbit.**

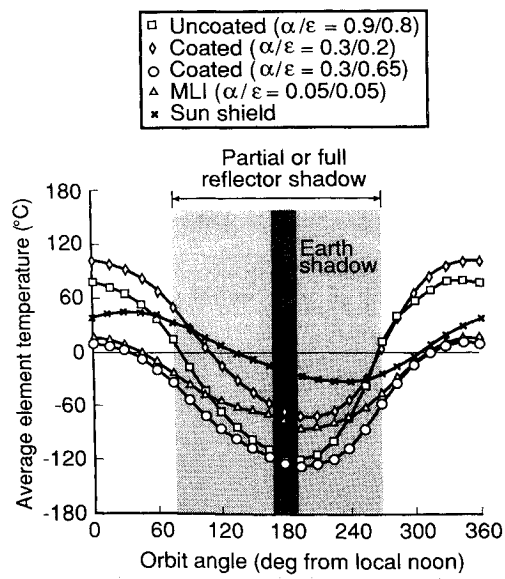


**Fig. 11 Average element temperature variation with orbit position—equinox orbit.**

tions. The baseline case has the greatest deviation in temperature, as expected, with the largest deviations occurring when the elements begin to enter and exit the reflector shadow (the two peaks in Fig. 12). The two coated cases also have large temperature deviations during these periods. The magnitudes of the two coated profiles were similar, with the high-ratio coating having slightly higher deviations. For the MLI, the extremely low effective surface properties limit the increases during the entire orbit. Temperature deviations for the Sun shield are also quite low, peaking when the minimum projected area faces the Sun (orbit positions of 75 and 255 deg).

**Distortion Analysis**

As the temperatures of the truss elements change throughout the orbit, the elements expand or contract depending on their thermal expansion properties and the change in element temperature relative to its undeformed temperature (22°C for this analysis). The distortion of an element also depends on the distortions of the nearby elements (and, thus, their temperatures). A linear-static structural analysis was performed to calculate the thermal distortions of the reflector support structure and assess their effect on antenna performance. The resulting nodal displacements experienced by the truss structure at each orbit position were obtained.

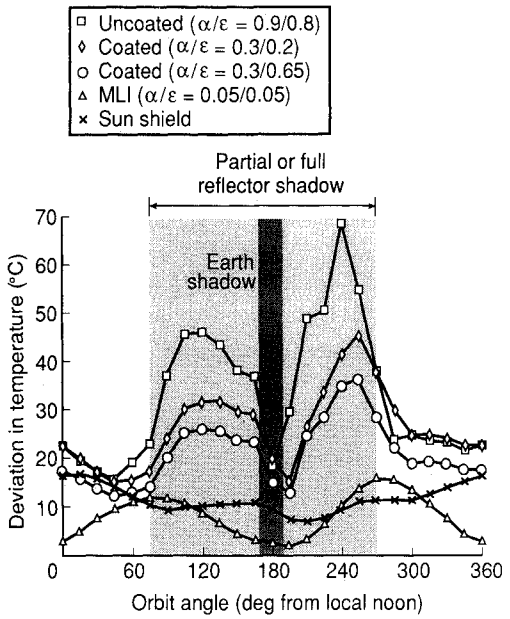


**Fig. 12 Mean standard deviation in temperature with orbit position—equinox orbit.**

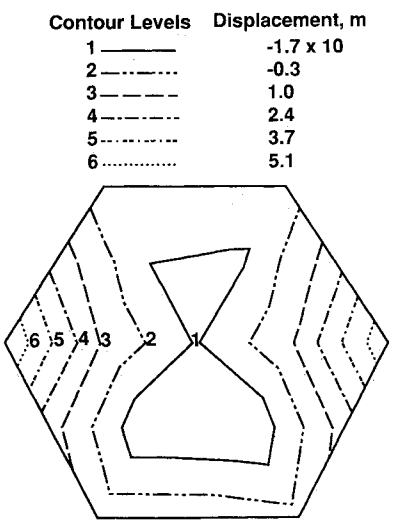


**Fig. 13 Surface contour of displacements along $z$ axis at an orbit position of 210 deg.**

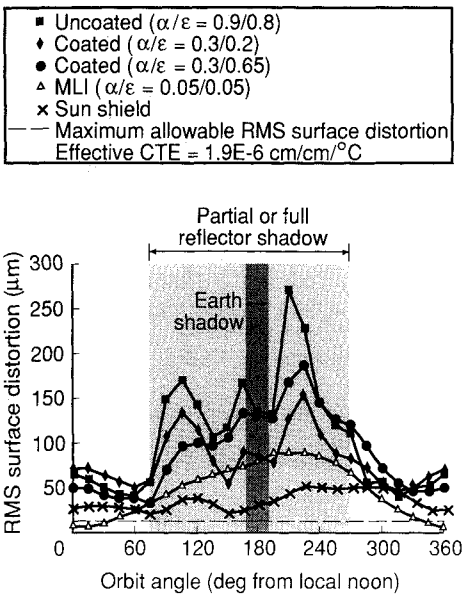


**Fig. 14 Reflector rms surface error variation with orbit position for five alternative thermal designs.**

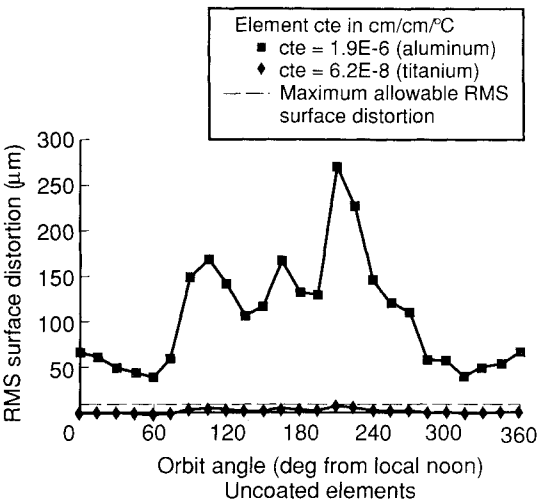


**Fig. 15 Root mean squared surface error vs orbit position for alternative end fitting materials.**

The $z$ components of a representative set of nodal displacements are shown on a simplified reflector surface in Fig. 13 to illustrate general distortion behavior. The contours shown were calculated for the uncoated truss at an orbit position of 210 deg. At this orbit position, the middle of the truss is shadowed by the reflector and is extremely cold, and the lower edge of the truss has moved from behind the reflector and is beginning to warm. These conditions cause the truss to curl toward the middle and to point slightly away from its proper direction. The severity of the distortions in both the middle and on the elevated side produce high overall distortions that lead to large rms distortion values. These translate into excessive scattering of the short-wavelength signal and reduced efficiency of the antenna.

*Root Mean Square Surface Distortion Comparisons*

Figure 14 shows the orbital variation in rms surface error due to the thermal distortion of the elements for the baseline and four alternative concepts. The figure illustrates the depen-

dence of the rms surface error on temperature characteristics of the various concepts. Two general trends are identified from these data. First, the majority of the large rms errors occur as the truss elements move behind the reflector and the average temperature drops. An example of this is the Sun shield concept where there appears to be direct inverse correlation between the shape of the average temperature profile (Fig. 11) and the shape of the rms error profile. Second, the largest errors occur most consistently when there is a strong mixture of shaded and unshaded elements, resulting in large temperature deviations (Fig. 12). These occur at the beginning and end of the shadow period. During the middle of the shadow period, average temperatures drop significantly while a few elements remain heated (causing the middle peak in the rms error profiles).

A line representing the surface accuracy requirement of this antenna (0.0136 mm) is included in Fig. 14. The baseline case exceeds this requirement by more than an order of magnitude as the reflector exits the shadow. The two coated cases exhibit trends similar in shape but significantly improved relative to the baseline case by virtue of the reduced temperature deviations across the truss throughout most of the orbit. The low-ratio coating works better than the high-ratio coating during Sun periods by maintaining lower element temperatures; its lower temperature deviations during the start of shadow translate to smaller rms errors. However, as the elements cool further during the shadow period, the extremely low temperatures lead to rms errors greater than those of the high-ratio coating. Unfortunately, neither option approaches the performance requirement.

The same is true for the MLI and Sun shade, although each greatly improves performance. Also, neither is prone to the erratic behavior associated with partial shadowing as are the baseline and the thermal-coating cases. The low emisssivity of the MLI prevents the drastic drops in temperature, while its low solar absorptivity lessens the heating effect of the Sun. On the other hand, the Sun shield always shadows the truss, preventing major oscillations in heating and cooling. Even though the MLI performs significantly better than the Sun shield in the reflector shadow, the Sun shield is the only option to partially meet the requirement (during part of the Sun period).

*Alternate Structural Materials*

As stated earlier, even the greatly reduced surface errors of the Sun shield and the MLI do not meet the 0.0136-mm (0.53-mil) rms requirement. One technique that may be necessary to meet this requirement is to actively control the surface with actuators attached to joints of each reflector panel. The application of this technology is beyond the scope of this paper.

Another approach is to employ elements with lower effective CTE values. Effective CTE values for elements depend on a number of factors including the type of material or composite used for the tubes and joints, the geometry of the material (e.g., the lay-up of the composites), and the length fraction of the tube and end fitting. The baseline structural concept, composed of unidirectional P75 graphite/epoxy composite tubes and two aluminum end fittings with a length fraction of 12.2%, had an element CTE of $1.9 \times 10^{-6}$ cm/cm/°C. Reducing the length of the joints reduces the element CTE substantially. However, constraints on the length of joints (manufacturing tolerances, astronaut and ground handling, and tube interface requirements) limit the extent to which they may be reduced. A more effective means is to select a joint material with a low CTE such as titanium (CTE = $8.28 \times 10^{-6}$ cm/cm/°C). Using the same length fraction, 12.2%, an effective element CTE of $6.2 \times 10^{-8}$ cm/cm/°C is obtained for the titanium joint, graphite-composite combination.

Figure 15 shows the orbital variation in rms surface error for the uncoated configurations for both the aluminum and titanium effective CTE values ($1.9 \times 10^{-6}$ and $6.2 \times 10^{-8}$ cm/cm/°C, respectively). It was assumed that small changes in the thermal conductivity and thermal capacitance of the end fittings would not noticeably change the temperatures calculated for the elements, therefore no new temperature profiles were calculated. This assumption is deemed valid since the conductivities and thermal capacitances of the two joint materials are similar. A linear relationship exists between element CTE and rms distortion, such that the reduction in CTE results in a linear reduction in rms surface error. As Fig. 15 shows, this reduction was sufficient to meet the surface accuracy requirement even for the worst uncoated heating and cooling conditions. Although not shown here, each of the other thermal options, when used in conjunction with the titanium joints, produces even better performance. This improved performance and the existence of on-orbit factors (e.g., radiation) that degrade unprotected graphite composites suggest that a combination of coating or insulation plus an element with an effective CTE of approximately $6.2 \times 10^{-8}$ cm/cm/°C is recommended for this type of high-accuracy large-diameter antenna structure. Additionally, since the manufacture of elements with an effective CTE value consistently approaching $6.2 \times 10^{-8}$ cm/cm/°C is still a challenge, the improved thermal performance offered by the use of coatings or insulation is critical.

## Concluding Remarks

A thermal-structural model was created, and analyses were conducted on a tetrahedral truss support for a 7.5-m-diam microwave radiometer antenna. Orbital variations in temperature were calculated and discussed. Root mean square surface errors were determined for five thermal protection alternatives.

Transient temperatures were shown to range from 150 to − 180°C, depending on orbit position and surface coating. The temperatures were strongly influenced by shadowing, particularly the shadow cast by the reflector surface. The effects of this shadow were evident throughout a large portion of both the equinox and solstice orbits. The shadow cast by the reflector was much more prominent than that cast by the Earth, such that results for both orbits were similar with only minor differences due to the presence of the Earth's shadow. Mixed success was achieved by the use of coatings in alleviating the various thermal problems. Although the coating with the lower absorptivity/emissivity ratio maintained temperatures within suggested material limits throughout the orbit, it allowed excessive temperature drops and thermal distortions during the shaded portions of the orbit. The coating with the high absorptivity/emissivity ratio reduced these distortions but allowed maximum temperatures to surpass suggested material limits during the sunlit periods. The Sun shield and the multilayer insulation performed better, both in maintaining moderate temperatures and in reducing distortions. However, these reduced distortions still exceeded the surface accuracy required for this mission.

Proper selection of end fitting materials to provide an effective element coefficient of thermal expansion near or below $1.0 \times 10^{-7}$ cm/cm/°C, coupled with application of truss element surface coatings with a low thermal emissivity and a low absorptivity/emissivity ratio (less than 1), can satisfy the rms surface accuracy requirements for frequencies at or below 220 GHz without the use of active surface control. Should thermoplastics be used, permitting higher temperatures, a higher ratio of absorptivity/emissivity can be more functional by allowing a more flexible choice of coatings. A Sun shield or multilayer insulation would provide improved surface accuracy and allow utilization of higher microwave frequencies.

## References

[1]Anon., "Geostationary Platform Bus Study for Earth Observation Sciences," Vol. II, Ford Aerospace Corp., WDL-TR11066, Contract NAS8-36104, Sept. 1987.

[2]Cosgrove, P. A., Farmer, J. T., and Rowell, L. F., "Thermal-Dis-

tortion Analysis of a Spacecraft Box Truss in Geostationary Orbit," NASA TP-3054, Nov. 1990.

[3]Wahls, D. M., Farmer, J. T., and Sleight, D. W., "On-Orbit Structural Dynamic Performance of a 15-Meter Microwave Radiometer Antenna," NASA TP-3041, Dec. 1990.

[4]Garrett, L. B., and Lovelace, U. M., "Large Space Systems Requirements, Deployable Concepts, and Technology Issues," American Astronomical Society, Paper 86-394, Washington, DC, October 1986.

[5]Hedgepeth, J. M., "Structures for Remotely Deployable Precision Antennas," NASA CR-182065, Jan. 1989.

[6]Collins, T. J., and Fichter, W. B., "Support Trusses for Large Precision Segmented Reflectors: Preliminary Design and Analysis," NASA TM-101560, March 1989.

[7]Leondis, A., "Large Advanced Space System Computer-Aided Design and Analysis Program," NASA CR-159191-1, July 1980.

[8]Anon., "Supertab—Engineering Analysis Pre- and Post-Processing User Guide," Structural Dynamic Research Corp., Millford, OH, 1988.

[9]Harris, A., and Pye, C., "TMG—Thermal Model Generator—A Thermal Analysis Computer Program—User's Guide," Revision 2.2, MAYA Heat Transfer Technologies, Ltd., Montreal, Quebec, Canada, 1988.

[10]Anon., "Supertab—Engineering Analysis Model Solution and Optimization User Guide" Structural Dynamic Research Corp., Millford, OH, 1988.

[11]Farmer, J. T., Wahls, D. M., and Wright, R. L., "Thermal-Distortion Analysis of an Antenna Strongback for Geosynchronous High Frequency Microwave Applications," NASA TP-3016, Sept. 1990.

Earl A. Thornton
*Associate Editor*